

# Bimetallic Mesoflowers: Region-Specific Overgrowth and Substrate Dependent Surface-Enhanced Raman Scattering at Single Particle Level

P. R. Sajanlal and T. Pradeep\*

*DST Unit on Nanoscience (DST UNS), Department of Chemistry and Sophisticated Analytical Instrument Facility, Indian Institute of Technology Madras, Chennai 600 036, India**Received December 11, 2009. Revised Manuscript Received February 10, 2010*

A strategy for the preparation of bimetallic mesoflowers (MFs) has been demonstrated by a simple overgrowth reaction. We make hybrid MFs containing Au core and shells of different metals, such as Ag and Pt, by tuning the experimental conditions so as to study region-specific overgrowth. This selective growth is attributed to the specific binding affinity of cetyltrimethylammonium bromide (CTAB) at different crystal planes of Au MF surfaces. We also studied the region-specific, composition dependent surface-enhanced Raman scattering (SERS) activity of single bimetallic MFs to understand their chemical environment. Substrate effects on the SERS activity at single particle level were evaluated by a comparative study of the Raman images of Au, Au/Ag, and Au/Pt MFs. Region-specific SERS activity exhibited by single Au/Ag MF provides an insight into the SERS activity of bimetallic MFs over their monometallic analogues.

## Introduction

In the world of nanoscience, architecture of intriguing objects with unusual size, shape, and properties has received enormous attention, and methods for the creation of such structures have been intensely explored. Incorporating chemical functionalities into nanoobjects is one way to tailor their physical and chemical properties, thereby making them useful for various applications in diverse areas.<sup>1</sup> Recent research has demonstrated methods to tune the properties of nanomaterials by incorporating multiple attributes into various one-, two-, and three-dimensional nanoobjects.<sup>2</sup> Making hybrid nanostructures with region-specific attributes is interesting in view of tailoring their properties at a single particle level.

To date, large numbers of nanoparticles with various shapes such as rod,<sup>3</sup> wire,<sup>4</sup> cube,<sup>5</sup> triangle,<sup>6</sup> star,<sup>7</sup> multipod,<sup>8</sup> and flower<sup>9</sup> have been reported. Hybrid nanoparticles are attractive because of the multifunctional properties arising due to different metal domains. Stripped nanowires made of different metal segments<sup>10</sup> with an increasing degree of complexity and functionality offer the possibility of selective functionalization of various regions within the same structure, with different molecules. Gold meso/nanoflowers (Au MFs)<sup>11</sup> are a new class of meso/nanoscale object developed recently in our group. These mesoflowers (MFs) have unique and highly anisotropic morphology, and it is possible to synthesize them in high yield. We demonstrated the utility of these nano/mesoscale objects in near-infrared (NIR)–infrared (IR) absorption and surface-enhanced Raman scattering (SERS).<sup>12</sup> The present work focuses on the incorporation of multiple functionalities into such a highly anisotropic mesomaterials in order to change the physical and chemical properties of the resulting structure.

Since it is hard to replicate the MF structures with unique morphology and inherent nanofeatures using metals other than Au, incorporation of desired metals to parent Au MFs by overgrowth is a way to create MFs of different composition. To some extent such hybrid materials can be used as a replica of the MFs of different metals if uniform overlayer is possible. Such structures with unique nanofeatures may provide novel properties. SERS is one such phenomenon which is highly dependent on the nature of the metal as well as size and shape of the nanoparticles. Since the SERS activity largely depends on the closeness of the Raman excitation wavelength and the surface plasmon resonance of the metal, all metals cannot act as good SERS substrates at certain excitation wavelengths. One of the effective ways to increase the SERS activity in transition metals other than coinage metals (Au, Ag, Cu) which show high SERS activity is to create a shell of weak SERS active transition metals around strong SERS active metal

\*Corresponding author: e-mail pradeep@iitm.ac.in; Fax + 91-44 2257-0545.

(1) (a) Cao, Y.-W.; Jin, R.; Mirkin, C. A. *J. Am. Chem. Soc.* **2001**, *123*, 7961. (b) Mallin, M. P.; Murphy, C. J. *Nano Lett.* **2002**, *2*, 1235. (c) Yang, J.; Lee, J. Y.; Chen, L. X.; Too, H.-P. *J. Phys. Chem. B* **2005**, *109*, 5468.

(2) (a) Suzuki, D.; Kawaguchi, H. *Langmuir* **2006**, *22*, 3818. (b) Chen, H. M.; Hsin, C. F.; Liu, R.-S.; Lee, J.-F.; Jang, L.-Y. *J. Phys. Chem. C* **2007**, *111*, 5909. (c) Hu, M.; Chen, J.; Marquez, M.; Xia, Y.; Hartland, G. V. *J. Phys. Chem. C* **2007**, *111*, 12558.

(3) (a) Liao, H.; Hafner, J. H. *Chem. Mater.* **2005**, *17*, 4636. (b) Kim, F.; Song, J. H.; Yang, P. D. *J. Am. Chem. Soc.* **2002**, *124*, 14316. (c) Sreeprasad, T. S.; Samal, A. K.; Pradeep, T. *Langmuir* **2007**, *23*, 9463. (d) Sau, T. K.; Murphy, C. J. *Langmuir* **2004**, *20*, 6414. (e) Sau, T. K.; Gole, A. M.; Orendorff, C. J.; Gao, J.; Gou, L.; Hunyadi, S. E.; Murphy, C. J. *J. Phys. Chem. B* **2005**, *109*, 13857. (f) Perez-Juste, J.; Pastoriza-Santos, I.; Liz-Marzán, L. M.; Mulvaney, P. *Coord. Chem. Rev.* **2005**, *249*, 1870–1901.

(4) (a) Hu, J. T.; Odom, T. W.; Lieber, C. M. *Acc. Chem. Res.* **1999**, *32*, 435. (b) Wiley, B.; Sun, Y.; Mayers, B.; Xia, Y. *Chem.—Eur. J.* **2005**, *11*, 454. (c) Sun, Y.; Xia, Y. *Science* **2002**, *298*, 2176. (d) Pei, L.; Mori, K.; Adachi, M. *Langmuir* **2004**, *20*, 7837. (e) Minelli, C.; Hinderling, C.; Heinzelmann, H.; Pugin, R.; Liley, M. *Langmuir* **2005**, *21*, 7080.

(5) Sun, Y.; Xia, Y. *Science* **2002**, *298*, 2176.

(6) (a) Shankar, S. S.; Rai, A.; Ankamwar, B.; Singh, A.; Ahmad, A.; Sastry, M. *Nat. Mater.* **2004**, *3*, 482. (b) Millstone, J. E.; Park, S.; Shuford, K. L.; Qin, L.; Schatz, G. C.; Mirkin, C. A. *J. Am. Chem. Soc.* **2005**, *127*, 5312. (c) Sajanlal, P. R.; Pradeep, T. *Adv. Mater.* **2008**, *20*, 980.

(7) (a) Nehl, C. L.; Liao, H. W.; Hafner, J. H. *Nano Lett.* **2006**, *6*, 683. (b) Kumar, P. S.; Pastoriza-Santos, I.; Rodríguez-González, B.; García de Abajo, F. J.; Liz-Marzán, L. M. *Nanotechnology* **2008**, *19*, 15606.

(8) Hao, E.; Bailey, R. C.; Schatz, G. C.; Hupp, J. T.; Li, S. *Nano Lett.* **2004**, *4*, 327.

(9) (a) Jena, B. K.; Raj, C. R. *Chem. Mater.* **2008**, *20*, 3546. (b) Bakshi, M. S.; Possmayer, F.; Petersen, N. O. *J. Phys. Chem. C* **2007**, *111*, 14113. (c) Li, Y.; Shi, G. *J. Phys. Chem. B* **2005**, *109*, 23787. (d) Jena, B. K.; Raj, C. R. *Langmuir* **2007**, *23*, 4064. (e) Wang, W.; Cui, H. *J. Phys. Chem. C* **2008**, *112*, 10759. (f) Qian, L.; Yang, X. *J. Phys. Chem. B* **2006**, *110*, 16672. (g) Yang, Z.; Lin, Z. H.; Tang, C. Y.; Chang, H. T. *Nanotechnology* **2007**, *18*, 255606.

(10) Keating, C. D.; Natan, M. J. *Adv. Mater.* **2003**, *15*, 451.

(11) Sajanlal, P. R.; Pradeep, T. *Nano Res.* **2009**, *2*, 306.

(12) (a) Kneipp, K.; Moskovits, M.; Kneipp, H. *Surface-Enhanced Raman Scattering: Physics and Applications*; Springer: Berlin, 2006. (b) Kneipp, K.; Kneipp, H.; Itzkan, I.; Dasari, R. R.; Feld, M. S. *Chem. Rev.* **1999**, *99*, 2957. (c) Campion, A.; Kambhampati, P. *Chem. Soc. Rev.* **1998**, *27*, 241. (d) Wang, H.; Levin, C. S.; Halas, N. J. *J. Am. Chem. Soc.* **2005**, *127*, 14992.

nanoparticles. Core-shell and alloy nanoparticles<sup>13</sup> belong to an important class of hybrid nanomaterials which can show excellent SERS property compared to their monometal analogues.<sup>14,15</sup> Because of the lower enhancement at the Au surface in the visible region compared to Ag,<sup>16</sup> synthesis of bimetallic nanostructures made of Au/Ag has been an active area of research for making good SERS active substrates. As a result, there have been many attempts to obtain core-shell particles by depositing Ag on preformed Au particles.<sup>17</sup> Formation of such hybrid materials largely depends on the interfacial energy between the two materials and the similarity in their lattice parameters.<sup>18</sup> So, epitaxial growth is one possible way to grow one metal over the other. It has been reported that the selective overgrowth of various metals on gold nanoparticles occurs by careful reduction of one metal over the other by playing with the reaction conditions.<sup>19</sup> While SERS is important, it is desirable to make core-shell nanoparticles with Pt shell in view of its specific chemical activity. Moreover, Pt can act as a nucleation center for the synthesis of magnetic nanoparticles.<sup>20</sup>

We report here a method for the formation of hybrid MFs by suitably adjusting the experimental conditions so as to create a shell of different metals such as Ag and Pt around Au MFs. We studied the region-specific overgrowth of Ag on Au MF in detail. A comparative study of the SERS activity of Au, Au/Ag, and Au/Pt MFs at the single particle level was conducted by analyzing the Raman images of individual MF particles using crystal violet (CV) as the Raman probe.

### Experimental Details

**Materials.** Tetrachloroauric acid trihydrate ( $\text{HAuCl}_4 \cdot 3\text{H}_2\text{O}$ ), cetyltrimethylammonium bromide (CTAB), ascorbic acid, and  $\text{AgNO}_3$  were purchased from CDH, India. Crystal violet and hexachloroplatinic acid ( $\text{H}_2\text{PtCl}_6 \cdot 6\text{H}_2\text{O}$ ) were purchased from Sigma-Aldrich. All chemicals were used as such without further purification. Triply distilled water was used throughout the experiments.

**Synthesis of Bimetallic Au MFs.** The Au MFs were synthesized as per our earlier procedure.<sup>11</sup> Briefly, 20 mL of CTAB (100 mM) was taken in a beaker, and 335  $\mu\text{L}$  of  $\text{Au}^{3+}$  (25 mM), 125  $\mu\text{L}$  of  $\text{AgNO}_3$  (10 mM), and 135  $\mu\text{L}$  of ascorbic acid (100 mM) were added sequentially. To this solution, 2 mL of Au/oligoaniline nanoparticles synthesized as per our earlier report<sup>21</sup> was added, and the solution was maintained at 80 °C for 1 h. It is then allowed to cool to room temperature. After 1 h, the solution was centrifuged at 3500 rpm for 4 min. The residue was washed with water three times in order to remove excess CTAB and other unwanted

materials. The slight yellowish residue of Au MFs was redispersed in 20 mL of deionized water. The effective concentration of Au in the MF dispersion is 0.418 mM, assuming a yield of 100%.

Ag overcoating was done by the reduction of Ag ions on Au MFs using ascorbic acid. The reaction was carried out in the absence and presence of surfactant, CTAB. For the selective overgrowth of Ag at the tip of the Au MFs, 5 mL of the Au MFs synthesized as per the above-mentioned procedure was added to a solution containing 1 mL of 100 mM CTAB, 2 mL of  $\text{AgNO}_3$  (10 mM), and 500  $\mu\text{L}$  of ascorbic acid (100 mM). Finally, 50  $\mu\text{L}$  of 250 mM NaOH solution was added slowly. This solution was kept at room temperature for 3 h. After that, the solution was centrifuged at 3000 rpm for 5 min. Subsequently, the whitish-gray residue was redispersed in distilled water and again centrifuged. This process was repeated three times in order to remove the unreacted ions present in the solution. The same reaction was repeated for 3 h in the absence of CTAB by keeping all other parameters constant.

In order to make the Pt-coated MFs, 5 mL of the as synthesized MFs was treated with 1 mL of 100 mM CTAB, 2 mL of 50 mM  $\text{H}_2\text{PtCl}_6$ , and 500  $\mu\text{L}$  of ascorbic acid (100 mM). This solution was kept at room temperature for 5 h. After that, the solution was centrifuged at 2000 rpm for 5 min. The black residue was redispersed in distilled water and centrifuged. This process was repeated three times in order to remove the unreacted ions and smaller Pt nanoparticles formed during this process.

**Instrumentation.** Scanning electron microscopic (SEM) images and energy dispersive analysis of X-ray (EDAX) studies were done with a FEI QUANTA-200 SEM. Field-emission scanning electron microscopic (FESEM) measurements were carried out using an FEI Nova NanoSEM 600 instrument. For SEM measurements, samples were drop-casted onto an indium tin oxide (ITO)-coated conducting glass and dried. Transmission electron microscopy (TEM) was carried out using a JEOL 3011, 300 kV instrument with an ultrahigh-resolution (UHR) pole piece. The samples for TEM were prepared by dropping the dispersion onto amorphous carbon films supported on a copper grid and dried in ambience. For Raman studies, the material was carefully transferred onto a cover glass and dried in ambience. Then the MF-coated glass plates were immersed in crystal violet solution ( $10^{-6}$  M) for 3 h. It was then washed carefully with water, dried, and mounted on the sample stage of the confocal Raman microscope. Raman imaging of the MF was done with a WiTec GmbH, Alpha-SNOM CRM 200 confocal Raman microscope having a 532 nm laser as the excitation source. A supernotch filter placed in the path of the signal effectively cuts off the excitation radiation. The signal was then dispersed using a 600 grooves/mm grating, and the dispersed light was collected by a Peltier cooled charge coupled device (CCD). For Raman imaging, the desired area was partitioned into 15 625 squares (an imaginary  $125 \times 125$  matrix drawn over it), with each square representing a sampling point and consequently a pixel for the image. Typical signal acquisition time at each pixel of the image was 50 ms. Intensities of the desired portion of the spectra collected over all the pixels were compared by Scan CTRL Spectroscopy Plus Version 1.32 software to construct a color-coded image. XPS measurements were done with Omicrometer ESCA Probe spectrometer with unmonochromatized  $\text{Al K}\alpha$  X-rays ( $h\nu = 1486.6$  eV). The samples were spotted as drop-cast films on the sample stub and dried in a vacuum desiccator. X-ray flux was adjusted to reduce the beam-induced damage of the sample. The energy resolution of the spectrometer was set at 0.1 eV at a pass energy of 20 eV for typical measurements.

### Results and Discussion

For the present study, we first synthesized uniform gold MFs as per our earlier report.<sup>11</sup> A large area SEM image of the parent gold MFs presented in Figure 1A shows that the synthesis yields MFs in very good yield and structural purity. The FESEM image

(13) (a) Xue, C.; Millstone, J. E.; Li, S.; Mirkin, C. *Angew. Chem., Int. Ed.* **2007**, *46*, 8436. (b) Sanedrin, R. G.; Georganopoulou, D. G.; Park, S.; Mirkin, C. A. *Adv. Mater.* **2005**, *17*, 1027. (c) Kim, C.; Kim, K. L.; Lee, S. J. *Chem. Phys. Lett.* **2005**, *403*, 77. (d) Sandhyarani, N.; Pradeep, T. *Chem. Mater.* **2000**, *12*, 1755.

(14) Gunawidjaja, R.; Peleshanko, S.; Ko, K.; Tsukruk, V. *Adv. Mater.* **2008**, *20*, 1544.

(15) (a) Nie, S.; Emory, S. R. *Science* **1997**, *275*, 1102. (b) Kneipp, K.; Wang, Y.; Kneipp, H.; Perelman, L. T.; Itzkan, L.; Dasari, R. R.; Feld, M. S. *Phys. Rev. Lett.* **1997**, *78*, 1667.

(16) Laserna, J. J. *Anal. Chim. Acta* **1993**, *283*, 607.

(17) (a) Freeman, R. G.; Hommer, M. B.; Grabar, K. C.; Jackson, M. A.; Natan, M. J. *J. Phys. Chem.* **1996**, *100*, 718. (b) Jana, N. R. *Analyst* **2003**, *128*, 954. (c) Selvakannan, P. R.; Swami, A.; Srisathyanarayanan, D.; Shirude, P. S.; Pasricha, R.; Mandale, A. B.; Sastry, M. *Langmuir* **2004**, *20*, 7825.

(18) Cozzoli, P. D.; Pellegrino, T.; Manna, L. *Chem. Soc. Rev.* **2006**, *35*, 1195.

(19) (a) Habas, S. E.; Lee, H.; Radmilovic, V.; Somorjai, G. A.; Yang, P. *Nat. Mater.* **2007**, *6*, 692. (b) Burda, C.; Chen, X.; Narayanan, R.; El-Sayed, M. A. *Chem. Rev.* **2005**, *105*, 1025. (c) Sajanlal, P. R.; Pradeep, T. *Langmuir* **2009**, DOI: 10.1021/la9020542.

(20) (a) Farrell, R. D.; Majetich, S.; Wilcoxon, J. *J. Phys. Chem. B* **2003**, *107*, 11022. (b) Grzelczak, M.; Rodríguez-González, B.; Pérez-Juste, J.; Liz-Marzán, L. M. *Adv. Mater.* **2007**, *19*, 2262.

(21) Sajanlal, P. R.; Sreerasad, T. S.; Nair, A. S.; Pradeep, T. *Langmuir* **2008**, *24*, 4607.

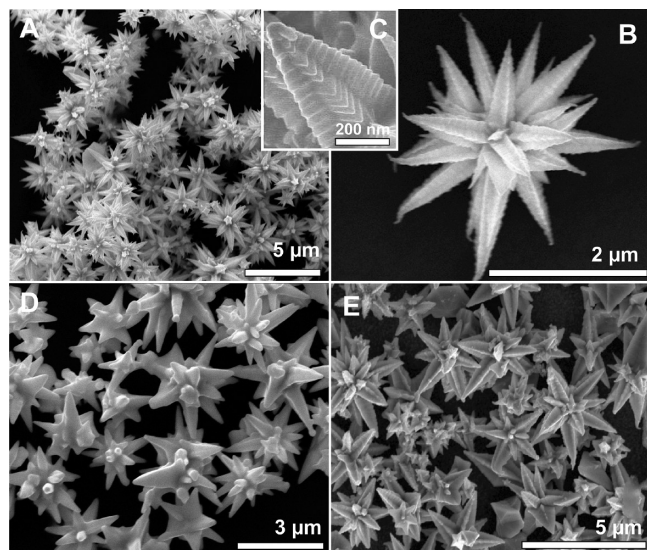


**Figure 1.** Large area SEM images of (A) Au MFs, (D) Au/Ag MFs, and (E) Au/Pt MFs. (B) and (C) are FESEM images of a single MF and a high-magnification view of a single stem, respectively.

of a single particle (Figure 1B) reveals the unique and complex morphology of the MF. Figure 1C shows a high-magnification FESEM image of a single stem. The scale-like feature on the MF is clearly visible in the image. These MFs were used for the subsequent overgrowth of Ag and Pt resulting in bimetallic MFs. Large area SEM images of Au/Ag and Au/Pt MFs formed are shown in parts D and E of Figure 1, respectively. Even though smaller nanoparticles of Ag and Pt are formed during this overgrowth process, all MFs have undergone the overgrowth reaction, resulting in the formation of Au/Ag and Au/Pt core–shell MFs which was evident from the SEM and TEM analyses. It is clear from the large area images that the flower-like morphology is retained in each MF after overgrowth, although the sharpness of the features reduced in the Au/Ag case.

The overgrowth was performed in such a way to control the deposition of Ag onto the surface of Au MFs. An FESEM image of a single bimetallic MF of Au core and Ag shell is shown in Figure 2A. When the Ag overgrowth was carried out in the presence of CTAB, a selective overgrowth was observed at the tip of the MFs compared to the other parts of the stem. Apart from this, we observed the nucleation of silver on specific areas of the surface of Au MFs. This is clear from Figure 2A. Ag nucleation was more evident at the tip of almost all the stems of the MFs. One major observation was the disappearance of the characteristic scale-like features of the stem of the MF. Even though these scale-like features were retained to some extent as small ridges and depressions on the body, it was totally absent at the tips of the MFs which were perfectly smooth after the overgrowth, confirming the pronounced coating at the tip. This region-specific overgrowth at the tip compared to the length of the stem was further confirmed from the elemental map of a single MF. The region-specific overgrowth in presence of the surfactant is attributed to the specific binding affinity of CTAB at different crystal planes. Silver overcoating was almost uniform when the overgrowth was carried out in the absence of CTAB, by keeping all other experimental parameters constant. The SEM image and corresponding EDAX images of the Au/Ag MF formed under this condition are shown in Supporting Information Figure S1.

As the EDAX image (Figure 2B) shows, the extent of Ag overgrowth was prominent at the tip compared to the center of

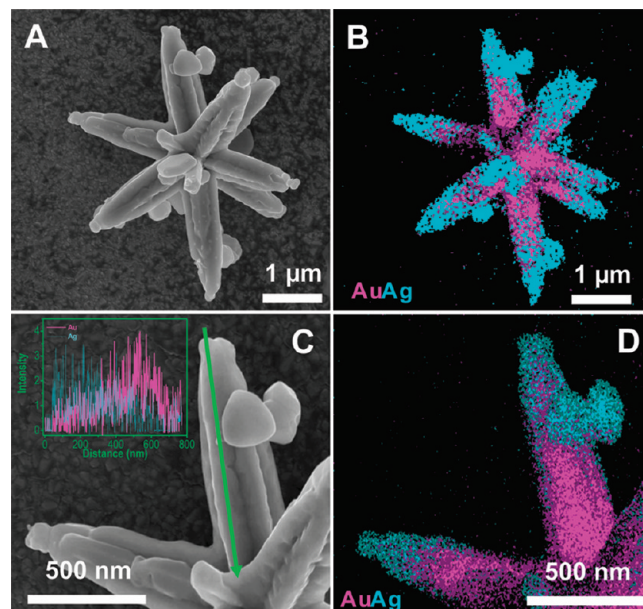


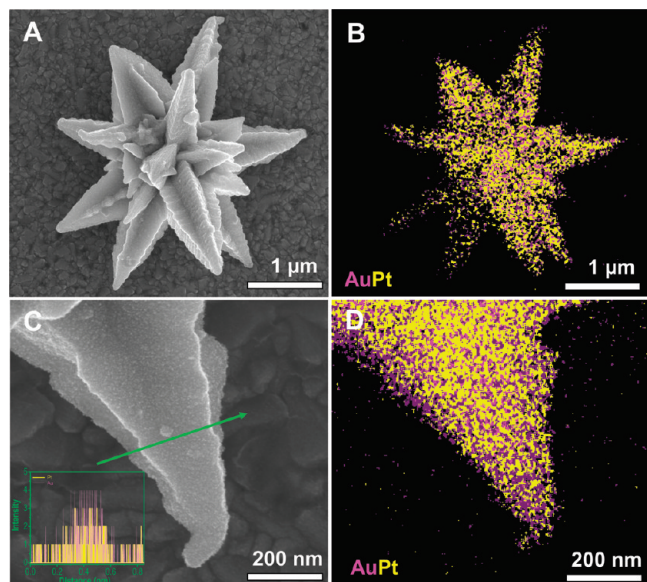
**Figure 2.** (A, B) FESEM and EDAX images, respectively, of a single Au/Ag bimetallic MF. (C) Magnified FESEM image of the stems of the Au/Ag MF and (D) corresponding EDAX image. Inset of (C) shows the line profile of the elements taken along the direction shown by the arrow. The elemental profiles are shown in different colors.

the Au MFs. An enlarged view of the stem of this MF is given in Figure 2C. The smoothness of the surface devoid of any scale-like appearance, in contrast to the parent Au MF, is clear from the SEM image. The corresponding EDAX image (Figure 2D) shows the elemental distribution on the Au MF surface. The line profile (inset of Figure 2C) taken along the stem of the MF, marked in Figure 2C, reveals the distribution of Au and Ag throughout the stem. High intensity of Ag at the tip compared to the body confirms the region-specific overgrowth of Ag on the Au surface. The EDAX spectrum collected from a single bimetallic MF is in agreement with the chemical composition expected (see Supporting Information Figure S2).

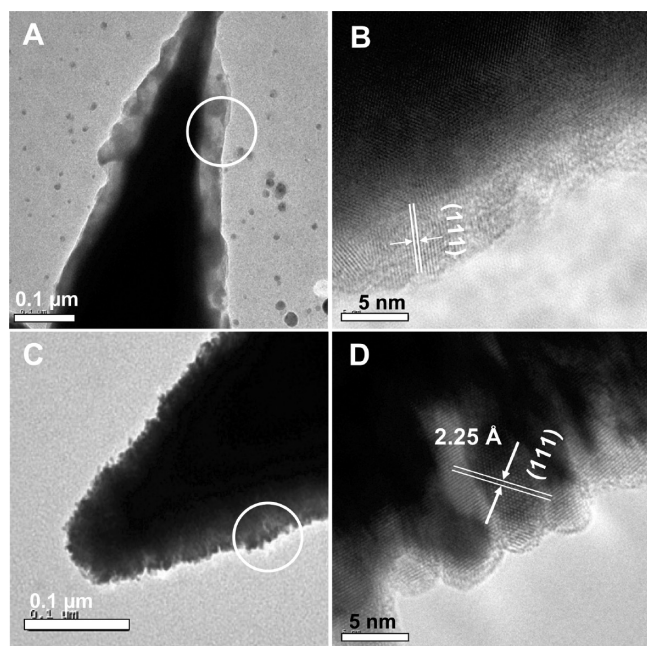
In the case of Pt, apparently the overcoating was not region specific, and the entire part of the MF was coated with Pt. Uniformity in coating was observed even in the thinnest coating, conducted for shorter times. Figure 3A shows the SEM image of a single Pt-coated Au MF. Pt distribution on the MF surface was confirmed from the EDAX image of the bimetallic Au/Pt MF. Overgrowth of Pt on the MF resulted in the roughening of its surface. This was clear from the enlarged SEM image of the stem of the MF (Figure 3C). Pt is well-known for its dendritic growth.<sup>22</sup> Careful examination of the surface of the stem reveals the dendritic overgrowth of Pt on Au MF (Figure 3C). The EDAX image of the tip of the MF reveals that the overgrowth is uniform and not region specific. The EDAX spectrum collected from Au/Pt MF is shown in Supporting Information Figure S3. The intensities of Au and Pt obtained from the line profile analysis (inset of Figure 3C) confirmed the uniform distribution of Pt on the Au MF surface.

Figure 4A shows the TEM image captured from the tip of an Au/Ag bimetallic MF. A thick coating of Ag at the tip of the stem was clearly visible from the image. This is marked in one part of the image (marked with a circle). Since both Au and Ag are having almost similar lattice parameters, Ag can grow epitaxially on the

(22) Song, Y.; Dorin, R. M.; Garcia, R. M.; Jiang, Y.-B.; Wang, H.; Li, P.; Qiu, Y.; Swol, F. v.; Miller, J. E.; Shelnutt, J. A. *J. Am. Chem. Soc.* **2008**, *130*, 12602.



**Figure 3.** (A, B) FESEM and EDAX images, respectively, of a single Au/Pt bimetallic MF. (C) SEM image of the stem of the Au/Pt MF and (D) corresponding EDAX image. Inset of (C) shows the line profile of the elements taken along the direction shown by the arrow. The elemental profiles are shown in different colors.



**Figure 4.** TEM images of tips of Au/Ag and Au/Pt MFs at different magnifications. (A) and (B) are respectively images of the tip and lattice resolved image of Au/Ag MF. (C) and (D) are respectively the tip and lattice resolved view of Au/Pt MF.

surface of Au MF. However, there are also regions where such growth is not observed. Because of similarity of the lattice constants, Ag cannot be distinguished from Au from the lattice resolved image (Figure 4B) alone. A thick coating of Ag (with lighter contrast) over Au MF (darker contrast) can be easily identified in the images (Figure 4A,B). The measured  $d$  spacing of 2.34 Å corresponds to the (111) plane of the surface coating of Ag. It is likely that some Ag nanoparticles nucleated in the solution by the reduction of  $\text{Ag}^+$  ions by ascorbic acid also adsorb on the surface of Au/Ag MFs. The presence of such particles is clear

from the TEM image (Figure 4A). They may be growing to larger particles as seen in Figure 2A.

It was observed that Ag overgrowth led to drastic changes of the MF surface when reduction was carried out at a higher concentration of ascorbic acid (500 mM). Instead of undergoing a region-specific reduction, the entire MF was reacted and gradually eaten away and was transformed to large number of bigger necklace-like and spherical nanoparticles (see Supporting Information Figure S4). We could also isolate various stages of degradation of the MFs (see Supporting Information Figure S4). The Ag overgrowth was clearly visible as small blisters (see Supporting Information Figure S4) on the surface of Au MF, at the early stages of the overgrowth. A high magnification image of a single stem shows the partially eaten stems. There was no selectivity in the overgrowth at this condition, and the entire body of the MF has undergone reaction. This indicates that the region-specific overgrowth is also dependent on the concentration of the reducing agent. It is believed that the ascorbate monoanion, formed by the reaction between NaOH and ascorbic acid, is facilitating the reduction of the Ag ions.<sup>23</sup> At higher concentration of ascorbic acid, a large number of ascorbate anions formed in the solution can enhance the nucleation of Ag throughout the entire body of the MF. At this condition, forced reduction of Ag may alter the crystal structure of the Au MF, leading to the degradation of the stems. Since the reaction was fast, we could isolate only a few such individual MFs. MFs at various stages of their degradation were identified, and composition of each structure was analyzed. SEM images, their corresponding Au  $M\alpha$  and Ag  $L\alpha$  based EDAX images, EDAX spectra, and quantification data of these structures are shown in Supporting Information Figure S5. As the extent of Ag nucleation increases, a reduction in the Au concentration and simultaneous increase in the Ag concentration was clearly seen in the EDAX spectra and quantification data. The Ag nucleation, thereby the Au MF degradation, results in the formation of necklace-like Ag nanoparticles. The presence of Au inside the Ag necklace-like structure (see Supporting Information Figure S5) indicates that Ag overgrowth happens from the Au nuclei.

In the case of Pt, the overgrowth happened in a dendritic fashion so as to form a thick, uniform coating of Pt on the entire body of the MF (Figure 4C). During the Pt overgrowth, the color of the MF solution changed to black. As in the case of Ag overgrowth, smaller Pt nanoparticles were also formed in the solution during overgrowth. Since the size of these nanoparticles was too small, we could easily separate them from bimetallic Au/Pt MFs by centrifugation. The measured  $d$  spacing of 2.25 Å shown in Figure 4D corresponds to the (111) plane of fcc Pt. Here, the growth happens mainly through the reduction of Pt(IV)–CTAB micelles<sup>24</sup> at the surface of Au MF by the electrons provided by ascorbic acid. The rate of Pt reduction at the Au MF surface would depend on the collision frequency between Pt(IV)–CTAB micelles and Au MFs. Unlike in the case of Au/Ag, no incorporation of spherical particles was observed for Au/Pt. When the overgrowth was conducted at higher concentration of ascorbic acid (500 mM), almost all the scale-like texture present on the surface of the parent MF disappeared. This is clear from the SEM images (see Supporting Information Figure S6). At this condition, the extent of overgrowth was very high, and more amounts of Pt ions underwent reduction and deposited on the surface of MFs.

(23) Jana, N. R.; Gearheart, L.; Murphy, C. J. *Chem. Commun.* **2001**, 617.

(24) Grzelczak, M.; Pérez-Juste, J.; González, B. R.; Liz-Marzán, L. M. *J. Mater. Chem.* **2006**, *16*, 3946.

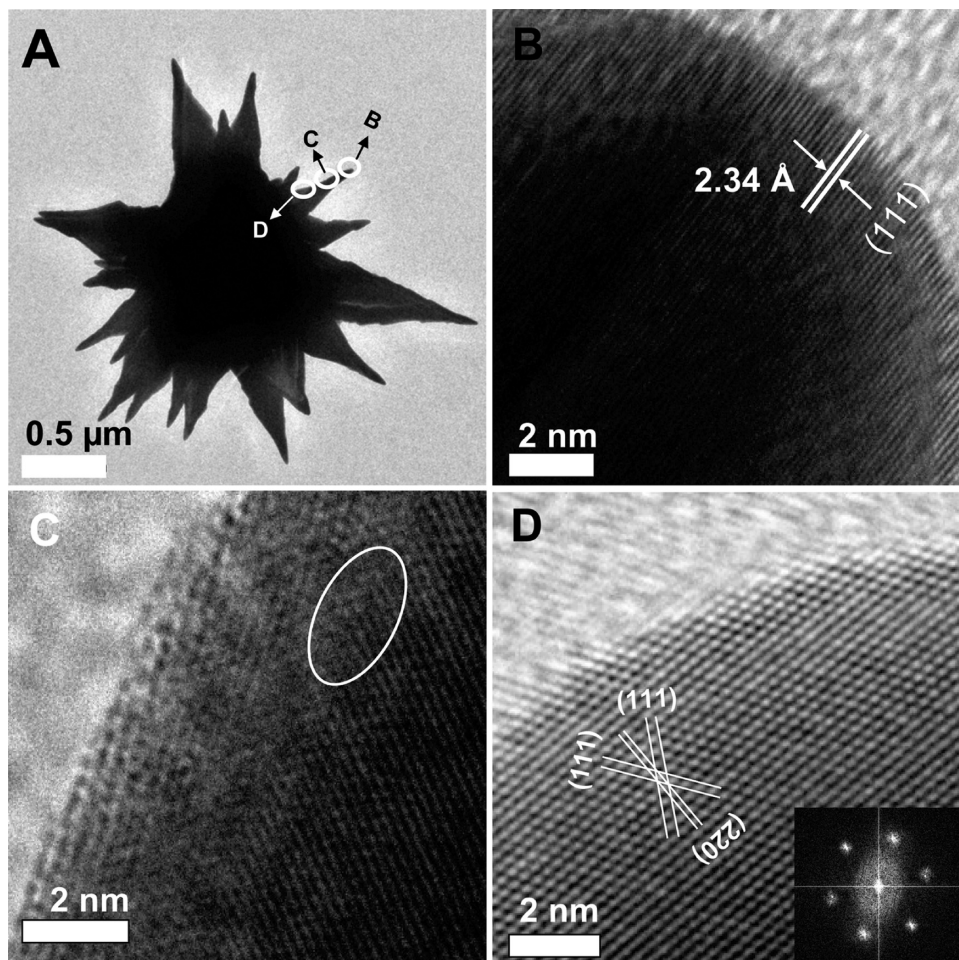


**Figure 5.** (A) TEM image of a single Au MF. (B)–(D) are the lattice-resolved images collected from respective areas of the stem marked in (A). Inset of (D) is a two-dimensional FFT image corresponding to (D).

In order to understand the reason for the site specific growth, we analyzed the parent Au MFs in detail. Figure 5 shows the TEM images of a single Au MF at different magnifications. From these studies it was found that the tip and tip edges of the MFs are composed of (111) planes, whereas the surface of the stem body is mainly comprised of (110) planes. The lattice spacing of 2.35 Å marked in Figure 5B,C corresponds to the (111) plane of gold. The lattice resolved image collected from the body edge of the Au MF is shown in Figure 5D, and the different planes are labeled in the image. The two-dimensional fast Fourier transform (FFT) image corresponding to Figure 5D is shown in its inset. The high reactivity at the tip of the MFs may be due to this structure. This can be explained by the following reasoning. The interatomic distance between the (110) planes in fcc gold is larger than in the other two common low index planes, (111) and (100).<sup>25</sup> Because of this reason, CTAB molecules will adsorb firmly to the less closely packed (110) planes compared to the other two low index planes. When the reaction was carried out in presence of CTAB, the overgrowth happened at the stable (111) facets, which were loosely protected by CTAB molecules. Thus, MFs are expected to have a high reactivity at the tip, which are composed of more (111) planes than the body. This was clear in the EDAX image. The structural modification at the body of the Au/Ag MF after the overgrowth and the EDAX data

reveal that the overgrowth happens at the body of MFs as well, but to a lesser extent.

The chemical compositions of Au and bimetallic MFs were further confirmed by X-ray photoelectron spectroscopy (XPS). Figure 6A shows the wide scan XPS spectra of parent and product MFs. The two states observed at ~83.9 and 87.8 eV in the enlarged XPS spectrum (Figure 6B) of Au MFs correspond to metallic Au 4f<sub>7/2</sub> and Au 4f<sub>5/2</sub> spin-orbit split states, respectively. In the case of Au/Ag and Au/Pt bimetallic MFs, the binding energies of Au 4f<sub>7/2</sub> and Au 4f<sub>5/2</sub> almost remained unchanged (Figure 6C,E) and were observed at ~83.9 and 87.8 eV. For the Au/Ag MFs, two peaks observed at 368.2 and 374.2 eV (Figure 6D) correspond to the binding energies of Ag 3d<sub>5/2</sub> and Ag 3d<sub>3/2</sub>, respectively. The peaks observed at 71.9 and 74.5 eV in Figure 6F correspond to Pt 4f<sub>7/2</sub> and Pt 4f<sub>5/2</sub> of Au/Pt MFs. The binding energies of Au, Ag, and Pt suggest metallic forms of the elements. Since the thickness of the surfactant coating present on the surface of Au MFs is very less, CTAB is unlikely to be present at the detection level of XPS as no Br feature was detected in XPS. However, the presence of Br on Au MFs was verified by the laser desorption ionization mass spectrometry (LDI MS).<sup>11</sup>

Since Au, Ag, and Pt nanoparticles are good SERS active substrates, it is expected that the hybrid materials made of any combination of nanoparticles of the above metals also exhibit SERS activity. It is known that the core-shell nanoparticles with

(25) Wang, Z. L.; Gao, R. P.; Nikoobakht, B.; El-Sayed, M. A. *J. Phys. Chem. B* 2000, 104, 5417.

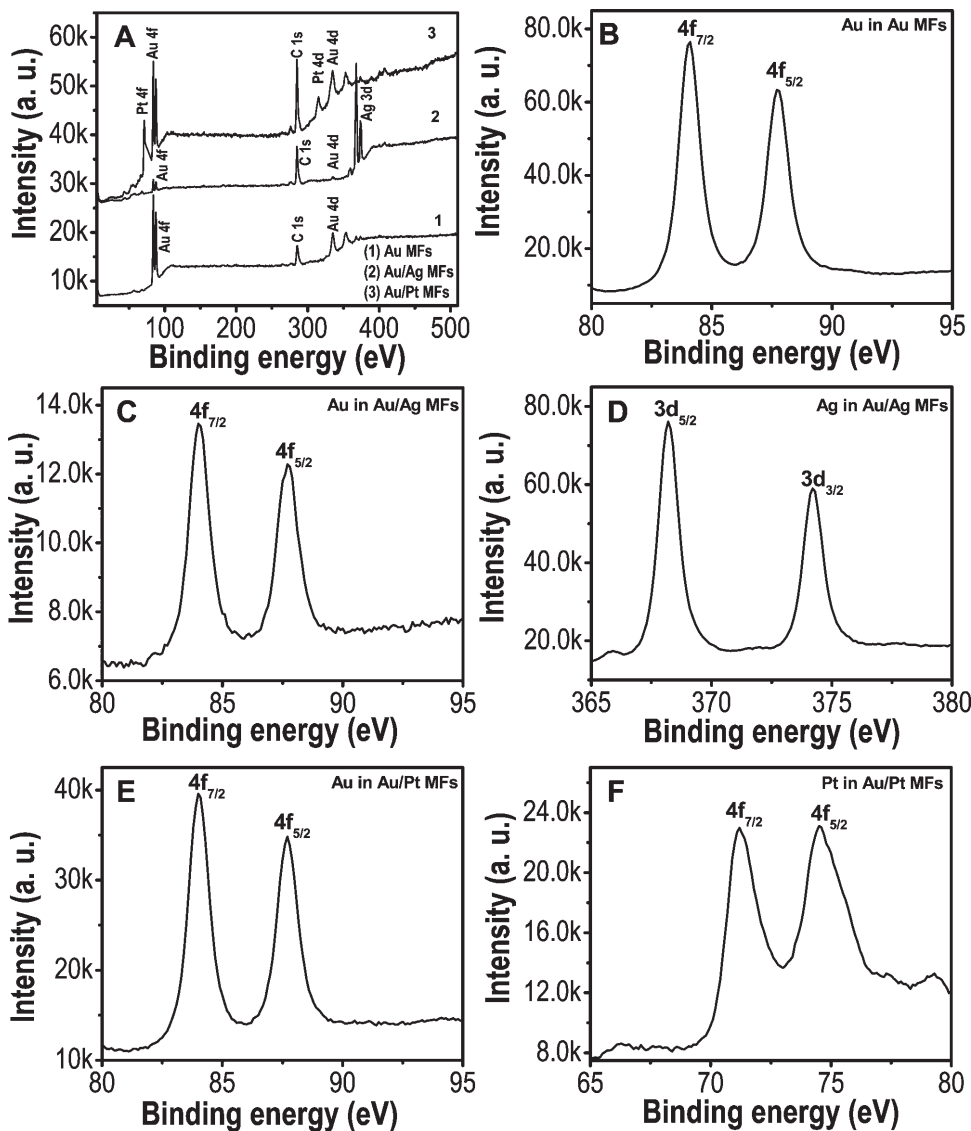


**Figure 6.** (A) Wide range XPS spectra collected from various MFs. (B), (C), and (E) are the XPS spectra of Au 4f region of Au, Au/Ag, and Au/Pt MFs, respectively. (D) and (F) are XPS spectra of Ag 3d and Pt 4f regions of Au/Ag and Au/Pt MFs, respectively.

Au core and Ag shell exhibit high SERS activity compared to their monometallic analogues.<sup>26,27</sup> Also, spiky tips and sharp edges can enhance the electric field around nanoparticles to a large extent.<sup>28</sup> We explored this aspect to understand the SERS activity of Au MFs in comparison to its hybrid core–shell MFs at single particle level, using Raman imaging. We performed Raman imaging of three different samples, Au, Au/Ag, and Au/Pt MFs, immobilized on separate glass slides which were immersed in CV solution of  $10^{-6}$  M for 5 h and were subsequently washed with distilled water. Throughout Raman imaging, the intensity of the laser was kept constant in order to compare the intensities of the SERS signals from the three different samples. Parts A–C of Figure 7 show the

Raman images of three different samples, Au, Au/Pt, and Au/Ag MFs, respectively. Corresponding optical images of the MFs selected for the Raman imaging are shown in the inset of the respective figures. We analyzed the intensities of Raman signals of adsorbed CV molecules on the MFs at two distinct areas, tip and body, of each MF. The Raman spectra collected from the tip and body (regions are encircled in each figure) of the monometallic and bimetallic MFs are presented in Figure 7D–F.

From the Raman images and spectra, it is clear that the SERS activity depends on the type of MFs used. In the case of Au MF, apart from a slight increase in the intensity at the tip of the stem (Figure 7D), it was almost the same throughout the entire area of the MF. The enhanced intensity at the tip can be attributed to the expected electric field enhancement at the sharp tips.<sup>7b,28</sup> The reason for the closeness of the Raman intensities at various areas of the Au MFs can be explained as follows. It is clear from the enlarged view of a single stem of the AuMF (Figure 1C) that the MF comprises of large number of star-shaped plate-like subunits stacked one over the other which gives a star-shaped appearance to the stem. An analyte molecule sitting in between two plate-like subunits or at the sharp ridges of the stem experience a large electric field. This can cause an increase in the intensity of their

(26) Sinfelt, J. H. *Acc. Chem. Res.* **1987**, *20*, 134.

(27) (a) Pande, S.; Ghosh, S. K.; Praharaj, S.; Panigrahi, S.; Basu, S.; Jana, S.; Pal, A.; Tsukuda, T.; Pal, T. *J. Phys. Chem. C* **2007**, *111*, 10806. (b) Henglein, A. *J. Phys. Chem. B* **1993**, *97*, 5457. (c) Pal, T.; Sau, T. K.; Jana, N. R. *Langmuir* **1997**, *13*, 1481.

(28) (a) Rodriguez-Lorenzo, L.; Alvarez-Puebla, R. A.; Pastoriza-Santos, I.; Mazzucco, S.; Stephan, O.; Kociak, M.; Liz-Marzan, L. M.; Garcia de Abajo, F. J. *J. Am. Chem. Soc.* **2009**, *131*, 4616–4618. (b) Myroshnychenko, V.; Rodriguez-Fernandez, J.; Pastoriza-Santos, I.; Funston, A. M.; Novo, C.; Mulvaney, P.; Liz-Marzan, L. M.; Garcia de Abajo, F. J. *Chem. Soc. Rev.* **2008**, *37*, 1792–1805. (c) Bakr, O. M.; Wunsch, B. H.; Stellacci, F. *Chem. Mater.* **2006**, *18*, 3297–3301. (d) Hao, F.; Nehl, C. L.; Hafner, J. H.; Nordlander, P. *Nano Lett.* **2007**, *7*, 729–732.

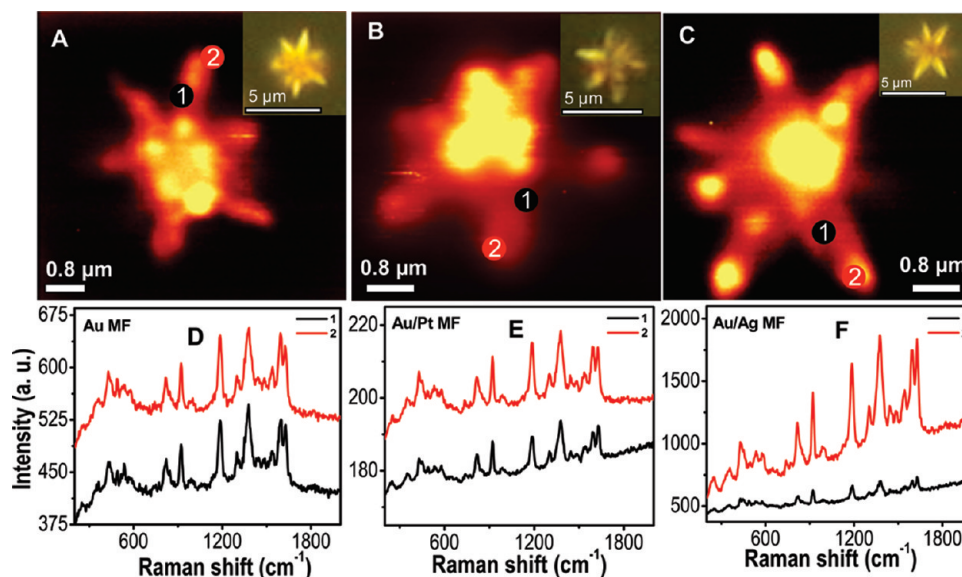


**Figure 7.** (A–C) Raman images of various MFs: (A) Au MF, (B) Au/Pt MF, and (C) Au/Ag MF. (D), (E), and (F) are the Raman spectra collected from the points marked in the images A, B, and C, respectively.

Raman signals. In the case of Pt-coated Au MFs, the SERS signals showed a reduction in intensity, which is pointing toward the low SERS activity of Pt compared to Au. The reduced SERS intensity of Au/Pt MF may be due to the larger difference in the Raman excitation wavelength and the surface plasmon of Pt. Even though Pt is a competitively low SERS active substrate than gold, the bimetallic Au/Pt MFs exhibited a good SERS intensity up to a concentration of  $10^{-6}$  M CV, probably due to the effect of the underlying Au core. Moreover, highly roughened, dendritic nature of the Pt shell will contribute to SERS as well.

In the case of Au/Ag MF, better SERS activity compared to bare Au MF was observed. Interestingly, we found a noticeable difference in the SERS intensity at the tip compared to the body of the Au/Ag MF. Increased intensity at the tip is attributed to the high Ag content at the tip, since Ag is a better SERS substrate than gold at this excitation wavelength ( $\lambda = 532$  nm). The expected electric field enhancement of spiky tips<sup>7b,28</sup> can also contribute to the high SERS activity at the tip. Since all stems are three-dimensional projections, a slightly different SERS intensity across the stem of the MFs is expected. This is due to the confocality of the instrument which collects Raman signals from a focal plane. However, such intensity differences are not high in the case of Au and Au/Pt MFs. For Au/Ag bimetallic MF alone, the situation is different and much larger SERS intensity is seen at the tip. Thus, the observed large difference is not due to the confocality of the measurement but due to a substrate effect. If confocality was responsible, the parent Au MFs also should have manifested similar effect as it has the same structure. Besides, the observed substrate dependent SERS activity was true for all the stems which were projecting in different directions. Increased intensity in Ag-rich regions can also be attributed to a charge transfer interaction between the ligand and

the Ag-coated Au substrate in view of the difference in electro-negativity of Au and Ag.<sup>27</sup>

## Conclusions

We synthesized bimetallic MFs made of gold core and silver/platinum shells through a directed overgrowth reaction. Region-specific overgrowth of silver over Au MFs was investigated. The differences in the surface structure of the MFs at the body and tip as well as the selective affinity of CTAB to specific planes are suggested to be the reasons for the selective overgrowth. In the case of Pt, a dendritic growth is seen. A comparative SERS study at single particle level was conducted to check the substrate effect on the SERS property. Region-specific SERS activity exhibited by Au/Ag MFs provides an insight into the SERS activity of bimetallic MFs over their monometallic analogues. High SERS activity of the bimetallic Au/Ag MFs and their unique shape would make them useful for related applications.

**Acknowledgment.** We thank Department of Science and Technology, Government of India, for constantly supporting our research program on nanomaterials.

**Supporting Information Available:** EDAX image of Au/Ag MF synthesized in the absence of CTAB; EDAX spectra of Au/Ag and Au/Pt MFs; SEM, EDAX images, EDAX spectra, and quantification data showing the shape transformation of MFs during Ag overgrowth at a higher concentration of ascorbic acid; and SEM images of Au/Pt MFs prepared at higher concentration of ascorbic acid. This material is available free of charge via the Internet at <http://pubs.acs.org>.